Side-dependent effect in the response of valve endothelial cells to bidirectional shear stress

Emilie Faure[1], Eric Bertrand[2], Amélie Gasté[1], Elise Plaindoux[1], Valérie Deplano[2,], Stéphane Zaffran[1,*]*

[1] Aix Marseille Univ, INSERM, Marseille Medical Genetics, U1251, 13005 Marseille, France

[2] Aix Marseille Univ, CNRS, IRPHE, UMR7342, 13013 Marseille, France

* Corresponding authors- Stéphane Zaffran, PhD, Marseille Medical Genetics, Aix Marseille Université, Inserm U1251, Faculté de médecine, 27 Bd Jean Moulin, 13005 Marseille, France ; stephane.zaffran@univ-amu.fr ; and Valérie Deplano, PhD, IRPHE, Aix Marseille Université, CNRS UMR7342, Technopôle de Château Gombert, 49 rue Frédéric Joliot Curie, BP146, 13384 Marseille cedex, France ; valerie.deplano@univ-amu.fr

Running title- side-specific valve endothelial cell response

Keywords- hemodynamic; aortic valve; valvular endothelial cells; wall shear stress

Abstract

Endothelial cells covering both sides (aortic and ventricular) of aortic valve leaflets are exposed to different stresses in particular the wall shear stress (WSS). Biomechanical stimuli actively regulate valve tissue structure and induce remodeling phenotype leading to valve dysfunction. For instance, endothelial to mesenchymal transformation (EndMT) is a process associated with aortic valve disease. The biomechanical response of cells at each sides of the aortic valve leaflets have not been clearly characterized. To analyze the mechanical response of valve endothelial cells (VECs) we developed unique fluid activation device that applies physiologically relevant pulsatile WSS (related to the belly, base and tip regions of the leaflet). We characterized the morphology and function of porcine aortic VECs derived from the opposite sides of aortic valve leaflets following exposure to different pulsatile WSS. We found that elongation and orientation of cells to pulsatile WSS depend on the side where they derived. Quantification of the gene expression confirms phenotype differences between aortic and ventricular VECs. Thus, aortic-VECs exposed to the pulsatile WSS related to the tip of the aortic side upregulated pro-EndMT (*ACTA2*, *Snail*, *TGFβ1*) and inflammation (*ICAM-1*, *VCAM-1*, *NFκB*) genes, whereas expression of endothelial markers like *PECAM*-1 was decreased. Conversely, ventricular-VECs showed strong increase of *PECAM-1* expression and no activation of pro-EndMT marker. Finally, we found that stress genes are upregulated in the two cell types, with a higher transcriptional level observed in ventricular- compared to aortic-VECs. Therefore, using a device enables to apply physiological shear stress we demonstrated a phenotype differences of VECs derived from opposite sides of aortic valve leaflets.

Introduction

The aortic valve maintains the unidirectional blood flow between the left ventricle and the ascending aorta. The aortic valve leaflets are made up of three highly organized layers of extracellular matrix (ECM) populated by valve interstitial cells and covered by a monolayer of valve endothelial cells (VECs). The distinct layers of ECM within the leaflet are mainly composed of collagen fibers at the aortic side (*fibrosa*), elastin at the ventricular side (*ventricularis*) and proteoglycan and glycosaminoglycan (*spongiosa*) in between [1]. The composition of ECM components contributes to the structural and mechanical proprieties of the valve. Collagen provides tensile strength to the valve leaflet during opening and transfer the load to the aortic wall when the valve is closed [2]. The elastin facilitates the fast opening of the valve leaflet. The spongiosa absorbs shocks during cardiac cycle and also facilitates the relative internal rearrangements to protect valve from damages [3]. VECs surrounding the valve leaflets are critical to circulatory function and blood-tissue interaction. They can respond to changing stimuli by altering their normal functions [4]. Experimental studies have reported that aortic valve leaflets experience a wide range of wall shear stress (WSS) depending on the side and regions (the base, belly and tip regions) of the leaflets (Butcher and Nerem, 2007). While the ventricular side experiences a strong pulsatile unidirectional WSS, the aortic side experience a much lower recirculating WSS. Therefore, the WSS is one such mechanical stimulus that greatly differs on either sides of the valve leaflets, and plays an important role in this side-dependent disease [5, 6].

Thus, abnormal blood velocity and pressure can apply environmental changes, which will have consequences at the macro- to microscales promoting maladaptive tissue remodeling. Such mechanical stimuli can activate the VECs, which transduce this signal to a biochemical signal that regulates gene expression and/or protein secretion particularly the ECM components in the valve [7, 8].

At the macroscale, hemodynamic forces induce WSS on the side of the valve leaflets as well as deformations of the valve tissue under cyclic stretch. WSS modulates the functions of valve cells and impacts the physiology and pathologies of these cells [9]. Recent 3D fluid structure interaction valve numerical modeling has investigated the macroscopic scale temporal and regional WSS characteristics on aortic valve leaflets under physiological flow [10, 11]. These studies confirmed the side-specificity differences in WSS pulsatility and magnitude between the base, belly and tip of the leaflets. High WSS, essentially unidirectional and pulsatile, with values comprised between 46 and 70 dyne/cm^2 near the base and the belly and reaching 93 dyne/cm^2 at the tip of the leaflet were found on the ventricular side but one-order of magnitude lower and bidirectional on the aortic side.

Identifying how VECs respond to mechanical forces is critical to better understand aortic valve disease. The side-specific of valve disease such as calcification might be attributed to the inherent differences in the VECs lining the aortic and ventricular sides of valve leaflets [12]. Interestingly, a study shown that ~10% of VECs in human valve undergo endothelial to mesenchymal transformation (EndMT) during development decreasing to ~1% in adult valve, suggesting a heterogeneity in the phenotype of these cells [13]. Considering a side-dependent differences in VECs we designed and used an original fluid activation device as a bioreactor to apply controlled *in vivo* like WSS on the surface of the cells. The flow profile within the bioreactor was characterized both computationally and experimentally. Exposure of different pulsatile shear stress magnitudes to VECs confirmed a side-dependent effect. Porcine aortic VECs isolated from the two sides of the leaflets elongated and aligned differently according to the different pulsatile WSS applied. We also observed a side-dependent expression pattern reflecting a differential response of these cells to biomechanical forces. Our results showed that aortic-VECs undergo EndMT associated with a decrease of endothelial gene expression and an increase of inflammation genes, whereas expression of *PECAM-1* was highly increased in

ventricular-VECs. Therefore, using an original fluid activation device we highlight the side-specific phenotype of VECs lining on the two sides of the aortic valve leaflets. These data help to better understand how heterogeneity of VECs contributes to their function at the side of the valve under physiological and pathophysiological conditions.

Materials and Methods

Bioreactor design, development and functioning

A schema of the bioreactor constituted by an original homemade fluid activation device linked to a specific 2D flow chamber is shown in Figure 1. An upstream glass reservoir bottle with screw cap pressure compensation (0.2 and 0.45µm filters) contains the culture medium to perform the experiment (Figure 1A). Its volume quantity depends on the duration in which the valve cells are submitted to WSS. Two stainless steel syringes (kdScientific) of 4.85mm inside diameter and 168.7mm of overall length of barrel were used (Figure 1B). One of the two syringes, filled with medium before the beginning of the experiment, injects the medium within the 2D flow chamber under the signal sent by the computer driven engine. This syringe is emptied, whereas the other one, mechanically enslaved to it in an opposite manner, fills up. When the medium volume contained in one syringe tends to zero, a 3- way solenoid operated pinch valve (Bio-Chem, 100PD3MP12-02S) is automatically actuated. Meanwhile the second syringe, which is full, injects the medium into the flow chamber. C-flex tubing (3.2mm OD, 1.6mm ID, St Gobain) was used for the pinch valve. Doing so numerous medium refilling manipulations and potential contaminations were avoided during the experiment. A downstream glass reservoir bottle was connected to the flow chamber outlet to collect the medium. A special attention was paid to avoid air bubbles within the syringes, the tubulars, and the flow chamber.

A computer-controlled trio motion coordinator was used to drive a stepper motor (HS200-2231, Danaher motion) linked to a rolled ball screw (W1001MA-3PY-C3Z2, NSK). A gear ratio system was also added to improve displacements' accuracy. This set up, using preloaded rolled ball screws with 0mm of axial play and a stepper motor with a small rotor inertia (J=340 g cm^2) allowed to perform fast accelerations and decelerations with high accuracy.

The choice of the technical specificities used to move both syringes as well as the linking system between the engine and the syringes are the major key points that allow this original fluid activation set-up to reproduce the *in vivo* WSS to which the valve cells are exposed in a perfectly controlled manner (see below for the validation of the activation device).

This fluid activation device is actually more adapted than commercial systems to mimic the rapid changes in flow direction. It is able to master pulsatility, accelerations, decelerations and fast variations of the flowrate generating pathophysiological flow waveforms. This demonstrated its superiority in comparison to previous works [14-16] that use 2D flow chamber, plastic syringes and peristaltic pump that generated steady or oscillatory flows which are far from achieving hemodynamic conditions on valvular leaflets.

In order to impose controlled WSS on a surface we needed to master the flow behavior in a flow chamber. It is now well known that a 2D parallel plate flow chamber, with specific geometrical dimensions, permits such a control.

Assuming fully developed, laminar and incompressible flow, there exists an analytical relation between the imposed flow rate Q within the chamber and the WSS induced on its walls: $Q = \frac{WSSlh^2}{6\mu}$ where l, h and μ are the width, the thickness of the flow chamber and the fluid dynamic viscosity respectively. This relation remains true when assuming unsteady flow given the value of the frequency parameter. Consequently, $Q(t) = \frac{WSS(t)lh^2}{6\mu}$ (equation 1).

The designed flow chamber was composed of three parts (Figure 1A). The upper and lower covers, 10mm thick, were machined using plexiglass. In between, the flow chamber itself, l=21mm and L=90mm, was machined using a 250µm thickness Lexan 8010 film sheet; inlet and outlet diameters were of 4mm. The fourteen stainless steel screws used for assembling the three parts ensured the flow chamber leak-tight. Tygon™ tubing (3.2mm OD, 1.6mm ID, St Gobain) and connectors in polypropylene (Ark Plas Products™) were used to associate flow chamber to the activation device components.

As this flow chamber is 2D, it was important to include a 3D scaffold to culture the VECs, which did not change the shear stress at the flow chamber walls but allowed for a 3D cell culture environment. To do so, elliptical holes, with major and minor axis dimensions of 26mm X 9.8mm respectively and 2mm of depth, were machined within the lower cover of the flow chamber (Figure 1A). They were then filled with a 3D collagen gel. 3D collagen gels at a concentration of 1.5 mg/mL collagen type I were made by addition of Dulbecco's Modified Eagle's Medium (DMEM, Thermo Fischer Scientific), 10% fetal bovine serum (FBS, Thermo Fischer Scientific), 0.1M NaOH and rat tail collagen (10 mg/mL concentration, BD Biosciences). An aliquot of the collagen solution was pipetted into each well and allowed to gel for at least 1hr at 37°C in 5%CO_2. VECs were seeded on the surface of the 3D collagen gels. It is worth noting that the 3D collagen gel is not a model of the leaflet tissue, but a 3D cell culture environment.

The dynamic viscosity of the working medium fluid was measured using a rheometer HaakeMars III, fluid μ=0.945e^{-3} Pa.s. The entire set up was placed in an incubator and kept at 37°C and 5% CO_2 during all the experiments.

Porcine Aortic Valve Endothelial Cells Isolation and Culture

Porcine aortic valve endothelial cells (VECs) were isolated from the aortic or the ventricular side of the aortic valve leaflets as previously described (Butcher et al., 2004). Porcine hearts were gently donated by the "abattoir Saint-Saturnin-lès-Apt". Briefly, aortic valve leaflets were isolated and incubated in collagenase type II/DMEM (Life Technologies) for 3x7 min. After incubation cells were gently scrapped to isolated VECs from the two sides of the leaflets. After isolation aortic or ventricular VECs were seeded and cultured on flask coated with 50ul/mL rat collagen type I (10 mg/mL concentration, BD Biosciences). VECs were cultured at 37°C and 5% CO_2 in Endothelial Cell Growth Medium (Promocell) supplemented with manufacturer's

adjuvants and 5% FBS. Endothelial cell phenotype and morphology was confirmed at passage 3 (no expression of *ACTA2*), and cells were used at passages 3 to 6.

Immunohistochemistry

Cells on collagen gels were fixed in 4% buffered paraformaldehyde during 10 min at room temperature. Fixed cells were washed for 15 min three times with PBS and permeabilized with 0.2% Triton-X 100 (Sigma) in PBS for 10 min. Cells were washed another three times with PBS before a saturation with 3% BSA and 10% Fetal Bovine Serum (Life Technologies). Cells were incubated overnight with Phalloidin-iFluor 488 Reagent (F-actin; abcam) and DAPI (4',6-diamidino-2-phenylindole) was used at 300 nM as a counterstain to distinguish cell nuclei. Cells were photographed with a confocal LSM800 (Zeiss).

Morphology Analysis

10 representative confocal images were taken on static and exposed cells on 3D collagen I gels that were fixed and stained with Phalloidin-iFluor 488 Reagent. The images were analyzed using Image J2 software [17]. Images from gels exposed to WSS were aligned so that the image horizontal corresponded to the direction of flow. Using Morpholib plugins on Image J2 software, cell area and cell perimeter were analyzed. Orientation angle between the horizontal (flow direction) and the majority of F-actin filaments was also determined. Based on cell area (A) and cell perimeter (P), Elongation index (Elong I) and Circularity index (shape index - SI) of cells (static or exposed to the flow) were determined ($SI = 4 \pi A / P^2$ and $Elong I = P^2 / 4 \pi A$). Cell alignment was assessed using angle orientation data. Frequency of cells upon angle orientation between 0-90°C were analyzed using Matlab software. Angle 0° were used as reference to cell parallel with the flow and 90° as reference to cell perpendicular with the flow.

Angle orientation data from static conditions or cells exposed to fibrosa WSS (base, belly and tip) were represented in polar histogram obtained using Matlab software.

Real time quantitative PCR (qPCR)

Cells were first removed from the collagen gels. Cells were lysed on Trizol (Life Technologies) and RNAs were extracted using RNeasy mini Kit (Qiagen). Reverse transcriptions were performed by using first strand cDNA synthesis kit (Agilent) per manufacturer's instructions. LightCycler 480 SYBR Green I Master mix (Roche) was used for quantitative real-time qRT-PCR analysis with a LightCycler 480 (Roche) following the manufacturer's instructions.

Each experiment was performed with n≥3. Samples were normalized to *TBP* as endogenous housekeeping gene. mRNA expression levels for each gene were calculated using the comparative cycle threshold (ΔΔCT) method. Normalized expression levels in the static condition were set to 1.0. Primers used are listed in Table 1.

Statistical Analysis

All experiments were performed with n≥3. Data is expressed as mean ±SEM. Statistical significance was determined using Student's *t* test to compare variances. For non-parametric data, the Mann-Whitney test was used to calculate significance between the medians. A p value < 0.05 was considered statistically significant.

Results

During cardiac cycle, wall shear stress (WSS) is considered as one of the most important hemodynamic parameters for valve endothelial cells (VECs). Previous transcriptional analysis of VECs isolated from aortic valve leaflets have identified side-specific differences in VECs expression suggesting heterogeneity in the VEC phenotype [12, 18]. In order to assess the side-specificity of VECs phenotype we designed and developed an original fluid activation device able to apply a physiological controlled pulsatile WSS on the surface of VECs isolated from the opposite sides of the leaflets. The temporal evolutions of the WSS radial component obtained by Cao et al, 2016 (Figure 2A-C) at base, belly and tip regions of the aortic side of the leaflets have been then modeled thanks to this original fluid activation device [10].

To analyze the WSS amplitudes and waveforms, it was important to determine their amplitude WSS variation (ΔWSS) as well as their maximum, minimum and mean ($\overline{\mathrm{WSS}}$) values at base, belly and tip regions (Table 2).

Table 2 shows large amplitude WSS variations, more particularly at belly and tip regions. Both positive and negative WSS values are high comparing to the mean values and the radial WSS component temporal evolutions (Figure 2A-C) put into light a significant alternation between these positive and negative values. To capture more accurately this bidirectional oscillatory waveform, oscillatory shear index, $\mathrm{OSI} = \frac{1}{2}\left(1 - \frac{\left|\int_0^T \mathrm{WSS}\,\mathrm{dt}\right|}{\int_0^T |\mathrm{WSS}|\mathrm{dt}}\right)$, [19], was also calculated. |WSS| is the name of WSS and T, the period of cardiac cycle. This index, which is a hemodynamic factor related to oscillation flow, can vary from 0 to 0.5. When considering a WSS component, OSI will be equal to 0 if WSS is always positive and 0.5 if highly oscillatory. In the present study, we found OSI_{base}=0.38, OSI_{belly}=0.4 and OSI_{tip}=0.45. With such a high temporal oscillation of WSS during the cardiac cycle, it is obvious that VECs are exposed to strongly oscillating WSS signals far from static and steady flow conditions. In this latter case, we can

also note that it would not be appropriate to subject VECs to WSS mean values that are low comparing to maxima or minima values encountered.

Validation of the flow device

The flow rates were generated by controlling the displacements of the syringes, (D_s), using a computer. A direct relation exists between D_s and the fluid volume, ϑ_f, injected, by the syringe: $\vartheta_f = S_{sy}D_s$.with S_{sy} being the syringe section. Considering t_i the time of fluid injection Q(t) is derived by $Q(t) = \frac{\vartheta_f}{t_i} = \frac{S_{sy}D_s}{t_i}$ (equation 2).

To validate our original fluid activation device, it was therefore important to record the syringe-imposed displacements to assess their spatio-temporal accuracy. Three different WSS signals computed at base, belly and tip of the aortic side were extracted from results reported in Cao et al., 2016 (Figure 2A-C). Flow rates corresponding to these signals were then determined through equation (1) and associated displacements of the syringe calculated using equation (2). Figure 2 shows the comparison between syringe-imposed displacements to generate radial WSS signals related to the belly, base and tip of the aortic side and the measured ones using Solartron Metrology displacement sensors (Figure 2G-I). The results highlight that the fluid activation device is able to precisely reproduce the complex and fast displacement changes, which, in turn, induce the WSS changes occurring during the cardiac cycle.

Response of endothelial cells to mechanical environment

We investigated the orientation and shape of aortic and ventricular VECs (aortic-VECs and vent-VECs) following static culture or exposure to different pulsatile WSS as predicted in the belly, base and tip regions of the aortic side [10]. Under static conditions, we found no difference between aortic- and vent-VECs since the two cell types were randomly oriented (Figure 3). Following exposure to pulsatile WSS predicted in the tip region of aortic side of the leaflets, aortic-VECs did not display clear orientation. Cells were randomly oriented, as more

than 60% had the angle of orientation ranged from 30° and 60° (Figure 3A,B). Elongation and shape index showed that aortic-VECs were mainly rounded (Figure S1). However, ventricular-VECs exposed to a similar pulsatile WSS adopted azimuthal orientation (Figure 3C, D). We found that 60% of vent-VECs were orientated with the angle of orientation ranged from 45° and 90°. Cell shape index analysis revealed that at equal magnitude of pulsatile WSS, vent-VECs have a more elongated shape than aortic-VECs (Figure S1). Together these results suggest that VECs isolated from the opposite sides of aortic valve leaflets have different phenotype.

Side-dependent differential gene expression

To further investigate the phenotype of the two cell types we analyzed the expression of different markers after an exposure to different pulsatile WSS (related to the belly, base and tip regions of the aortic side). For the aortic-VECs we quantified changes in pro-EndMT (*ACTA2*, *Snail*, *TGFβ1*) genes following exposure to pulsatile WSS (Figure 4A). Compared to static control exposure to pulsatile WSS predicted in the tip region at the aortic side significantly upregulated pro-EndMT gene expression (*ACTA2* 4.3±0.3 fold increase over static control, $p<0.05$). Interestingly, the upregulation of *ACTA2* expression was proportional to the magnitude of the pulsatile WSS applied (Figure 4B). However, ventricular-VECs exposed to similar pulsatile WSS did not show comparable activation of *ACTA2* compared to aortic-VECs (Figure 4B). We further analyzed the expression of endothelial gene (*PECAM-1*) in the two cell types. Expression of *PECAM-1* was increased in aortic-VECs exposed to pulsatile WSS predicted in the base region of the aortic side of the leaflets (*PECAM-1* 3.2±0.7 fold increase over static control, $p<0.05$), whereas it was downregulated in cells exposed to pulsatile WSS predicted in the belly and tip regions (Figure 5A). Conversely, *PECAM-1* expression was strongly upregulated in ventricular-VECs after exposure to the three pulsatile WSS applied (Figure 5B). For instance, expression of *PECAM-1* was highly increased in vent-VECs exposed

to pulsatile WSS predicted in the tip region (*PECAM-1* 60±10 fold increase over static control, $p<0.05$). As activation of inflammatory mediators is induced by abnormal shear stress [20], we analyzed the expression of 2 inflammatory markers (*VCAM-1* and *ICAM-1*). Expression of these genes was upregulated in both cell types with some differences (Figure 6). Expression of *VCAM-1* and *ICAM-1* was increased in aortic-VECs with the highest activation in cells exposed to pulsatile WSS with the highest differential (Figure 6A; *ICAM-1* 49.5±3.7 fold increase after exposure as predicted in tip region over static control, $p<0.05$). Upregulation of *NFκB* expression in aortic-VECs confirmed the activation of inflammation in this cell type with (Figure S2). Although expression of *VCAM-1* and *ICAM-1* were both increased in vent-VECs (Figure 6), activation of *VCAM-1* was significantly stronger in this cell type compared to its upregulation in aortic-VECs (Figure 6B; *VCAM-1* 265±17 fold increase after exposure as predicted in tip region over static control, $p<0.05$). Thus, these results suggest that the pulsatile fibrosa WSS affects expression of inflammatory markers in the vent-VECs. To analyze the activation of stress-related genes in both cell types we quantified expression of *NRF-2* and *EGR-1*, which are known to respond to shear stress in endothelial cells [21, 22]. Expression of *NRF-2* and *EGR-1* was upregulated in the two cell types, but we found that activation of these two genes was stronger in vent-VECs compared to aortic-VECs (Figure 7A,B). Together these findings indicate that aortic- and vent-VECs behave differently to pulsatile WSS predicted in the different regions of the aortic side of aortic valve leaflets.

Discussion

Although the aortic valve is cover by a monolayer of endothelial cells at its two sides (aortic and ventricular) the phenotype of valve endothelial cells (VECs) to shear stress remains poorly understood. Here we utilized fluid activation device to show that VECs respond differently to similar WSS depending on the side where they originated. Shear stress is known to play a leading role in endothelial cell migration and hence, vessel remodeling. Shear stress has also been shown to result in directed migration of endothelial cells against the direction of flow [23]. Our findings showed differences in the alignment of aortic- vs vent-VECs to the direction of the flow. We found that the orientation angle of 60% of vent-VECs was ranged between 45° to 90° when magnitude of the pulsatile WSS was the highest (tip). Conversely, at a similar pulsatile WSS magnitude less aortic-VECs were oriented with this angle suggesting these two cell types align differently to the flow. The alignment behaviors that we observed in these two cell types may thus reflect a specific response to high WSS. The exact mechanism by which VECs sense shear stress remains unclear. Several endothelial cell flow sensors have been proposed for endothelial cells including integrin complexes, ion channels, caveolae and complex including PECAM-1, VE-cadherin and VEGFR2 [24]. Our observations suggest that the expression of *PECAM-1* was highly upregulated in vent-VECs compared to aortic-VECs confirming that cell-cell contacts may be implicated in flow sensing [25].

Several studies have also shown EndMT on the aortic side of adult valves, which is exposed to bidirectional shear stress and is often the site of inflammatory and calcific degeneration [26, 27]. On the contrary, EndMT is absent at the ventricular side of the valve [28]. At this side, the VECs are exposed to high unidirectional shear stress. We identified that bidirectional WSS signal induces EndMT in aortic-VECs whereas ventricular-VECs do not.

Our findings display that inflammatory markers (*VCAM-1* and *ICAM-1*) are upregulated in both populations of VECs in response to physiological bidirectional WSS. The difference of *VCAM-*

1 upregulation between the aortic- versus vent-VECs is consistent with a previous study showing differential expression of VCAM-1 on opposite sides of normal aortic valves [12]. The upregulation of *VCAM-1* and *ICAM-1* has already been demonstrated in response to TNF-α, suggested a role for the hemodynamic environment in valve inflammatory process [29]. However, our results differ to a previous study, which demonstrated that exposure of the aortic, but not ventricular, surface of the aortic valve leaflet to bidirectional shear stress increases expression of inflammatory markers [20]. The WSS signal used in this previous study, although bidirectional, was not physiological. More particularly the accelerating and decelerating slopes as well as the frequency of flow direction changes were lower than those physiologically observed. Another difference is that we used isolated VECs and not a leaflet. Therefore, cells within the endothelium, which cover the leaflets, may be less sensitive to shear stress than isolated cells. Indeed, it is known that the trilaminar structure of the leaflet protects the valve, and so the VECs, from its environment (hemodynamic and biomechanics). Although VECs were cultured directly on the collagen gel we observed that exposure to particular conditions induced EndMT and probably invasion in the matrix, however, the collagen gel has different stiffness than the ECM forming the leaflet tissue. Assessment of the effect of the difference in stiffness has demonstrated that valve cells phenotype responds to changes of the 3 D culture environments [30, 31]. Thus, it would be important to work on a 3D cell culture environment that reproduces the physiological condition.

Our results confirm a previous study showing that VECs on aortic and ventricular surfaces have differential gene expression profiles and, therefore, distinct phenotypes [12]. The observation of morphological and functional differences between VECs isolated from the two sides of aortic valve leaflets and exposed to identical conditions suggests that the side-specific phenotypic differences is in part intrinsic. Recent transcriptomic analysis of postnatal heart valves at single cell resolution demonstrated that the endothelial cell population is separated into three distinct

subpopulations that display specific spatial location in heart valve leaflets [18]. The VECs subset, which is characterized by classic endothelial markers, can be found on both sides of porcine aortic valve leaflets. However, a particular subset of VECs is present in regions of high mechanical stress, where valve leaflets are exposed to high shear [18]. Interestingly, a recent study demonstrated restricted expression of Wnt9b in endothelial layer of zebrafish heart valves in response to fluid forces [32]. Altogether these findings suggest a contribution of biomechanical forces to maintain VECs diversity in different region of the valves.

Conclusions

In the current study, we designed and developed unique fluid activation device that applies physiologically relevant pulsatile WSS (related to the belly, base and tip regions of the leaflet). We identified a clear phenotype difference between VECs isolated from the opposite sides of aortic valve leaflets. This model replicates the physiological radial component of WSS predicted in different regions of the aortic side of the aortic valve leaflet. We observed that aortic-VECs undergo EndMT when bidirectional WSS, characterized by high OSI value, is applied, whereas vent-VECs are less sensitive to this WSS feature. We found that VECs isolated from the two sides of aortic valve leaflets induced inflammatory process, which probably respond to the activation of a stress program. Our findings provide an improved understanding of phenotype differences of VECs to their environment and suggest that vent-VECs are less subject to valve disease.

Acknowledgments

We thank Dr. Gaëlle Odelin for her help in collecting pig hearts. This work was supported by the "Association Française contre les Myopathies" (TRIM-RD Project), and the "Institut National de la Santé et de la Recherche Médicale" to S.Z. E.F received a postdoctoral fellowship from the "Association Française contre les Myopathies" and the "Fondation Lefoulon Delalande".

Author Contributions: conceptualization, E.F., V.D. and S.Z.; validation, E.F. and E.B.; formal analysis, E.F., E.P., A.G.; investigation, S.Z.; writing—original draft preparation, V.D. and S.Z.; writing—review and editing, V.D. and S.Z.; supervision, S.Z.; funding acquisition, S.Z.

Conflicts of Interest: The authors declare no conflict of interest. The funders had no role in the design of the study; in the collection, analyses, or interpretation of data; in the writing of the manuscript, or in the decision to publish the results.

Figure legends

Figure 1: Schematic illustration of the fluid activation device. (A) Scheme illustration of the flow chamber. (B) Scheme of the bioreactor set-up for physiological wall shear stress experiments.

Figure 2: A unique fluid device system producing a pulsatile WSS. Comparison between imposed piston displacements to generate bidirectional WSS signals related to the belly of the *fibrosa* leaflet side and the measured ones using Solartron Metrology displacement sensors. It is clear that the fluid activation device is able to reproduce the complex and fast displacement changes inducing the WSS changes occurring during the cardiac cycle. (A,D,G) Radial WSS signals at belly, base and tip regions of the aortic side of the aortic valve leaflets from Cao et al, 2016. (B,E,H) Associated flow rates. (C,F,I) Comparison between the displacements imposed to generate the flow rates associated to the WSS (blue symbol) and the measured ones (black symbol).

Figure 3: Valve endothelial cell alignment following exposure of wall shear stress. (A-D) Valve endothelial cell (VECs) derived from opposite sides (aortic and ventricular) of aortic valve leaflets were cultured under static conditions or exposed to different pulsatile wall shear stress (WSS) as predicted in the base, belly and tip regions of the aortic side of the leaflets. (A,C) F-actin is shown in green; nuclei are labeled with DAPI (blue). Orientation angle of VECs was determined in static condition or following exposure of different pulsatile WSS and displayed as a rose plot to represent the frequency and directionality of the cells. Quantification of the angle between the nucleus and flow showed that 60% of vent-VECs aligned between 45° and 90° to the flow direction.

Figure 4: Valve endothelial cell phenotype following exposure of wall shear stress. (A) EndMT-related gene expression in valve endothelial cells (VECs) derived from the aortic side following exposure of pulsatile wall shear stress (WSS) related to tip region of the aortic side of aortic valve leaflets. (B) *ACTA-2* expression in VECs derived from opposite sides (aortic and ventricular) of aortic valve following exposure of different pulsatile WSS (as predicted in the base, belly and tip regions of the aortic side). qRT-PCR experiments were performed in triplicate (n= 3 for each conditions) and expressed as mean ±SEM (*p<0.05 using Mann-Whitney test). Normalized expression levels in the static condition were set to 1.

Figure 5: *PECAM-1* expression following exposure of wall shear stress. (A,B) *PECAM-1* expression in aortic-VECs (A) and ventricular-VECs (B) following exposure of different pulsatile WSS (as predicted in the base, belly and tip regions of the aortic side). qRT-PCR experiments were performed in triplicate (n= 3 for each conditions) and expressed as mean ±SEM (*p<0.05 using Mann-Whitney test). Normalized expression levels in the static condition were set to 1.

Figure 6: Expression of inflammatory markers after exposing valve endothelial cells to wall shear stress. *IVAM-1* and *VCAM-1* expression in VECs derived from opposite sides (aortic and ventricular) of aortic valve leaflets following exposure of different pulsatile WSS (as predicted in the base, belly and tip regions of the aortic side of aortic valve leaflets). qRT-PCR experiments were performed in triplicate (n= 3 for each conditions) and expressed as mean ±SEM (*p<0.05 using Mann-Whitney test). Normalized expression levels in the static condition were set to 1.

Figure 7: Expression of stress-related genes after exposing valve endothelial cells to wall shear stress. (A,B) *NRF-2* (A) and *EGR-1* (B) expression in VECs derived from opposite sides (aortic and ventricular) of aortic valve leaflets following exposure of different pulsatile WSS (as predicted in the base, belly and tip regions of the aortic side of aortic valve leaflets). In pulsatile WSS as predicted in the tip region the expression of *NRF-2* was 2.93±1 fold increased over static control ($p<0.05$) in aortic-VECs and 6.21±0.1 fold increased over static control ($p<0.05$) in vent-VECs. Similarly, in pulsatile WSS as predicted in the tip region the expression of *EGR-1* was 2.86±0.37 fold increased over static control ($p<0.05$) in aortic-VECs and 71.5±3 fold increased over static control ($p<0.05$) in vent-VECs. qRT-PCR experiments were performed in triplicate (n= 3 for each conditions) and expressed as mean ±SEM (*$p<0.05$ using Mann-Whitney test). Normalized expression levels in the static condition were set to 1.

References

[1] Hinton RB, Yutzey KE. Heart valve structure and function in development and disease. Annual review of physiology. 2011;73:29-46.
[2] Schoen FJ. Mechanisms of function and disease of natural and replacement heart valves. Annual review of pathology. 2012;7:161-83.
[3] Duan B, Kapetanovic E, Hockaday LA, Butcher JT. Three-dimensional printed trileaflet valve conduits using biological hydrogels and human valve interstitial cells. Acta biomaterialia. 2014;10:1836-46.
[4] Rabkin-Aikawa E, Mayer JE, Jr., Schoen FJ. Heart valve regeneration. Advances in biochemical engineering/biotechnology. 2005;94:141-79.
[5] Arjunon S, Rathan S, Jo H, Yoganathan AP. Aortic valve: mechanical environment and mechanobiology. Annals of biomedical engineering. 2013;41:1331-46.
[6] Holliday CJ, Ankeny RF, Jo H, Nerem RM. Discovery of shear- and side-specific mRNAs and miRNAs in human aortic valvular endothelial cells. American journal of physiology Heart and circulatory physiology. 2011;301:H856-67.
[7] Balachandran K, Sucosky P, Yoganathan AP. Hemodynamics and mechanobiology of aortic valve inflammation and calcification. International journal of inflammation. 2011;2011:263870.
[8] Steed E, Boselli F, Vermot J. Hemodynamics driven cardiac valve morphogenesis. Biochimica et biophysica acta. 2016;1863:1760-6.
[9] Butcher JT, Tressel S, Johnson T, Turner D, Sorescu G, Jo H, et al. Transcriptional profiles of valvular and vascular endothelial cells reveal phenotypic differences: influence of shear stress. Arteriosclerosis, thrombosis, and vascular biology. 2006;26:69-77.
[10] Cao K, Bukac M, Sucosky P. Three-dimensional macro-scale assessment of regional and temporal wall shear stress characteristics on aortic valve leaflets. Computer methods in biomechanics and biomedical engineering. 2016;19:603-13.
[11] Cao K, Sucosky P. Computational comparison of regional stress and deformation characteristics in tricuspid and bicuspid aortic valve leaflets. International journal for numerical methods in biomedical engineering. 2017;33.
[12] Simmons CA, Grant GR, Manduchi E, Davies PF. Spatial heterogeneity of endothelial phenotypes correlates with side-specific vulnerability to calcification in normal porcine aortic valves. Circulation research. 2005;96:792-9.
[13] Paruchuri S, Yang JH, Aikawa E, Melero-Martin JM, Khan ZA, Loukogeorgakis S, et al. Human pulmonary valve progenitor cells exhibit endothelial/mesenchymal plasticity in response to vascular endothelial growth factor-A and transforming growth factor-beta2. Circulation research. 2006;99:861-9.
[14] Butcher JT, Nerem RM. Porcine aortic valve interstitial cells in three-dimensional culture: comparison of phenotype with aortic smooth muscle cells. The Journal of heart valve disease. 2004;13:478-85; discussion 85-6.
[15] Butcher JT, Penrod AM, Garcia AJ, Nerem RM. Unique morphology and focal adhesion development of valvular endothelial cells in static and fluid flow environments. Arteriosclerosis, thrombosis, and vascular biology. 2004;24:1429-34.
[16] Mahler GJ, Frendl CM, Cao Q, Butcher JT. Effects of shear stress pattern and magnitude on mesenchymal transformation and invasion of aortic valve endothelial cells. Biotechnology and bioengineering. 2014;111:2326-37.
[17] Rueden CT, Schindelin J, Hiner MC, DeZonia BE, Walter AE, Arena ET, et al. ImageJ2: ImageJ for the next generation of scientific image data. BMC bioinformatics. 2017;18:529.

[18] Hulin A, Hortells L, Gomez-Stallons MV, O'Donnell A, Chetal K, Adam M, et al. Maturation of heart valve cell populations during postnatal remodeling. Development. 2019;146.
[19] Ku DN, Giddens DP, Zarins CK, Glagov S. Pulsatile flow and atherosclerosis in the human carotid bifurcation. Positive correlation between plaque location and low oscillating shear stress. Arteriosclerosis. 1985;5:293-302.
[20] Sucosky P, Balachandran K, Elhammali A, Jo H, Yoganathan AP. Altered shear stress stimulates upregulation of endothelial VCAM-1 and ICAM-1 in a BMP-4- and TGF-beta1-dependent pathway. Arteriosclerosis, thrombosis, and vascular biology. 2009;29:254-60.
[21] Havis E, Duprez D. EGR1 Transcription Factor is a Multifaceted Regulator of Matrix Production in Tendons and Other Connective Tissues. International journal of molecular sciences. 2020;21.
[22] Hosoya T, Maruyama A, Kang MI, Kawatani Y, Shibata T, Uchida K, et al. Differential responses of the Nrf2-Keap1 system to laminar and oscillatory shear stresses in endothelial cells. The Journal of biological chemistry. 2005;280:27244-50.
[23] Simmers MB, Pryor AW, Blackman BR. Arterial shear stress regulates endothelial cell-directed migration, polarity, and morphology in confluent monolayers. American journal of physiology Heart and circulatory physiology. 2007;293:H1937-46.
[24] Chatterjee S, Fisher AB. Mechanotransduction in the endothelium: role of membrane proteins and reactive oxygen species in sensing, transduction, and transmission of the signal with altered blood flow. Antioxidants & redox signaling. 2014;20:899-913.
[25] Conway DE, Breckenridge MT, Hinde E, Gratton E, Chen CS, Schwartz MA. Fluid shear stress on endothelial cells modulates mechanical tension across VE-cadherin and PECAM-1. Current biology : CB. 2013;23:1024-30.
[26] Mohler ER, 3rd. Mechanisms of aortic valve calcification. The American journal of cardiology. 2004;94:1396-402, A6.
[27] Mohler ER, 3rd, Gannon F, Reynolds C, Zimmerman R, Keane MG, Kaplan FS. Bone formation and inflammation in cardiac valves. Circulation. 2001;103:1522-8.
[28] Mahler GJ, Farrar EJ, Butcher JT. Inflammatory cytokines promote mesenchymal transformation in embryonic and adult valve endothelial cells. Arteriosclerosis, thrombosis, and vascular biology. 2013;33:121-30.
[29] Aikawa E, Whittaker P, Farber M, Mendelson K, Padera RF, Aikawa M, et al. Human semilunar cardiac valve remodeling by activated cells from fetus to adult: implications for postnatal adaptation, pathology, and tissue engineering. Circulation. 2006;113:1344-52.
[30] Duan B, Yin Z, Hockaday Kang L, Magin RL, Butcher JT. Active tissue stiffness modulation controls valve interstitial cell phenotype and osteogenic potential in 3D culture. Acta biomaterialia. 2016;36:42-54.
[31] Yip CY, Chen JH, Zhao R, Simmons CA. Calcification by valve interstitial cells is regulated by the stiffness of the extracellular matrix. Arteriosclerosis, thrombosis, and vascular biology. 2009;29:936-42.
[32] Goddard LM, Duchemin AL, Ramalingan H, Wu B, Chen M, Bamezai S, et al. Hemodynamic Forces Sculpt Developing Heart Valves through a KLF2-WNT9B Paracrine Signaling Axis. Developmental cell. 2017;43:274-89 e5.

Gene		Sequences
PECAM-1	Forward	5’ - ATCTGCATCTCGTGGGAAGT - 3’
	Reverse	5’ - GAGCTGAAGTGTCAGCAGGA - 3’
ICAM-1	Forward	5’ - AAAGGAGGCTCCATGAAGGT - 3’
	Reverse	5’ - TGCCATCGTTTTCCACATTA - 3’
VCAM-1	Forward	5’ - TTGTTTCCTCGTCACACAGC - 3’
	Reverse	5’ - CAATCTGCGCAATCATTTTG - 3’
eNOS	Forward	5’ - CTCCTGCCAGAGAGGATTTG - 3’
	Reverse	5’ - CACCCACATCCCCATCAC - 3’
ACTA2	Forward	5’ - TCCATCCTGGCCTCTCTGT - 3’
	Reverse	5’ - GCTTCGTCGTACTCCTGTT - 3’
EGR-1	Forward	5’ - CACCTTCCCCACACCTAATAC - 3’
	Reverse	5’ - CAGATAGTCAGGGATCATGGG - 3’
NRF-2	Forward	5’ - CATACGCAACAGGAAACACAG - 3’
	Reverse	5’ - GCCCATACAGAAGTTCAGACAG - 3’
Tgfß1	Forward	5’ - TTTCTGGTGGGGAGACAGAC - 3’
	Reverse	5’ - CTCCCCTAGGCTGCTTTCTT - 3’
Snail1	Forward	5’ - GCCCAACTACAGCGAGCTAC - 3’
	Reverse	5’ - CCAGGAGAGACTCCCAGATG - 3’
NFκB1	Forward	5’ - CTTTCGCAAACTCAGCTTCAC - 3’
	Reverse	5’ - CTTTGGTTTATGCGGTGTTGG - 3’
TBP	Forward	5’ - TGGACGTTCGGTTTAGGTTG - 3’
	Reverse	5’ - ACGAGCAACTTACAGGAACG - 3’

Table 1: Primers used for RT-PCR

Table 2: WSS characteristics predicted in the base, belly and tip of the leaflet (TSM is expressed in dyn/cm2,
TSG is expressed in dyn/cm2 s).

	Max(WSS)	Min(WSS)	ΔWSS	$\overline{WSS}$
Base	+5.67dyn/cm^2	-10.97dyn/cm^2	16.64dyn/cm^2	-0.33dyn/cm^2
Belly	+13.69dyn/cm^2	-11.86dyn/cm^2	25.56dyn/cm^2	0.36dyn/cm^2
Tip	+14.91dyn/cm^2	-9.25dyn/cm^2	24.16dyn/cm^2	0.20dyn/cm^2

A

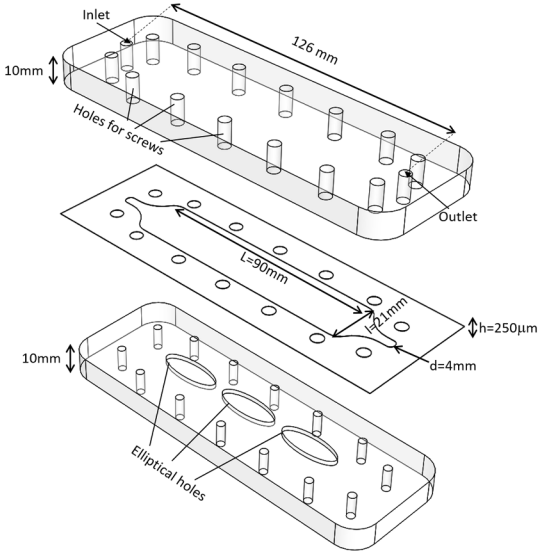
Inlet
126 mm
10mm
Holes for screws
Outlet
L=90mm
l=21mm
h=250µm
d=4mm
10mm
Elliptical holes

B

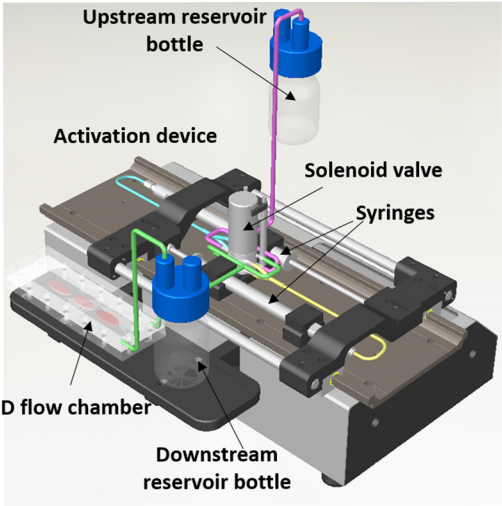
Upstream reservoir bottle
Activation device
Solenoid valve
Syringes
2D flow chamber
Downstream reservoir bottle

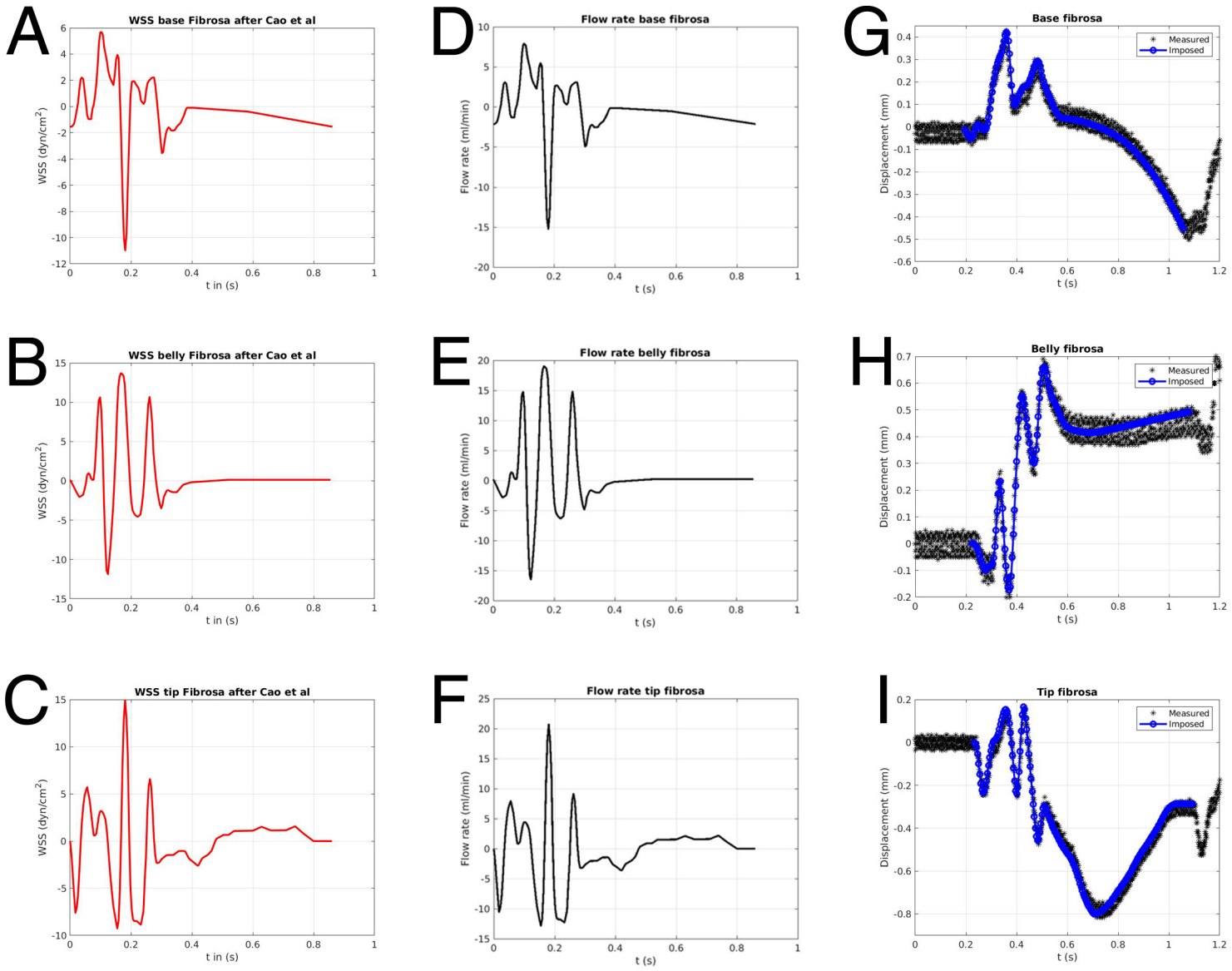
A
WSS base Fibrosa after Cao et al
WSS (dyn/cm^2)
t in (s)
B
WSS belly Fibrosa after Cao et al
WSS (dyn/cm^2)
t in (s)
C
WSS tip Fibrosa after Cao et al
WSS (dyn/cm^2)
t in (s)
D
Flow rate base fibrosa
Flow rate (ml/min)
t (s)
E
Flow rate belly fibrosa
Flow rate (ml/min)
t (s)
F
Flow rate tip fibrosa
Flow rate (ml/min)
t (s)
G
Base fibrosa
Measured
Imposed
Displacement (mm)
t (s)
H
Belly fibrosa
Measured
Imposed
Displacement (mm)
t (s)
I
Tip fibrosa
Measured
Imposed
Displacement (mm)
t (s)

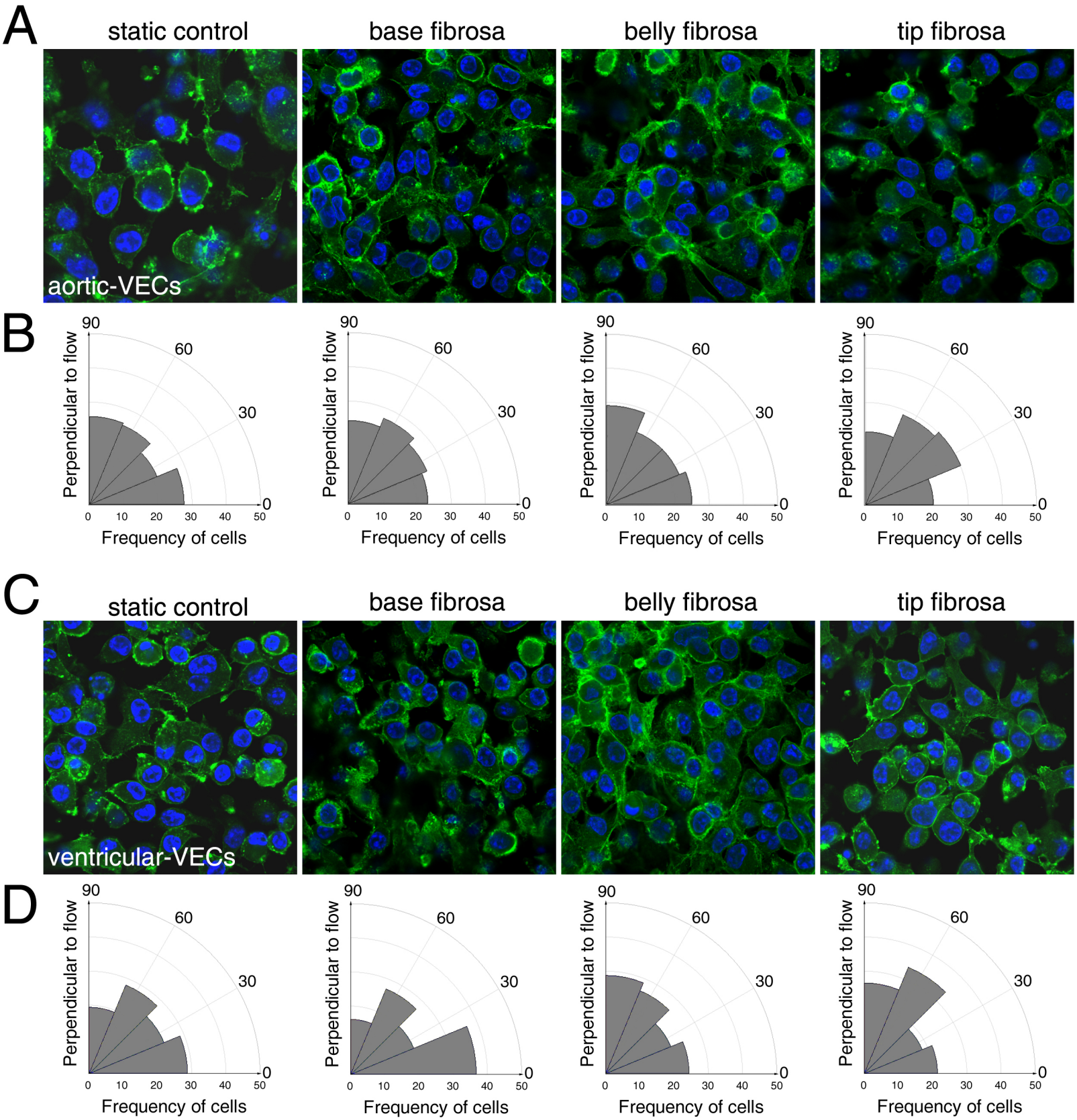
A
static control
base fibrosa
belly fibrosa
tip fibrosa
aortic-VECs
B
Perpendicular to flow
Frequency of cells
C
static control
base fibrosa
belly fibrosa
tip fibrosa
ventricular-VECs
D
Perpendicular to flow
Frequency of cells

Figure 3

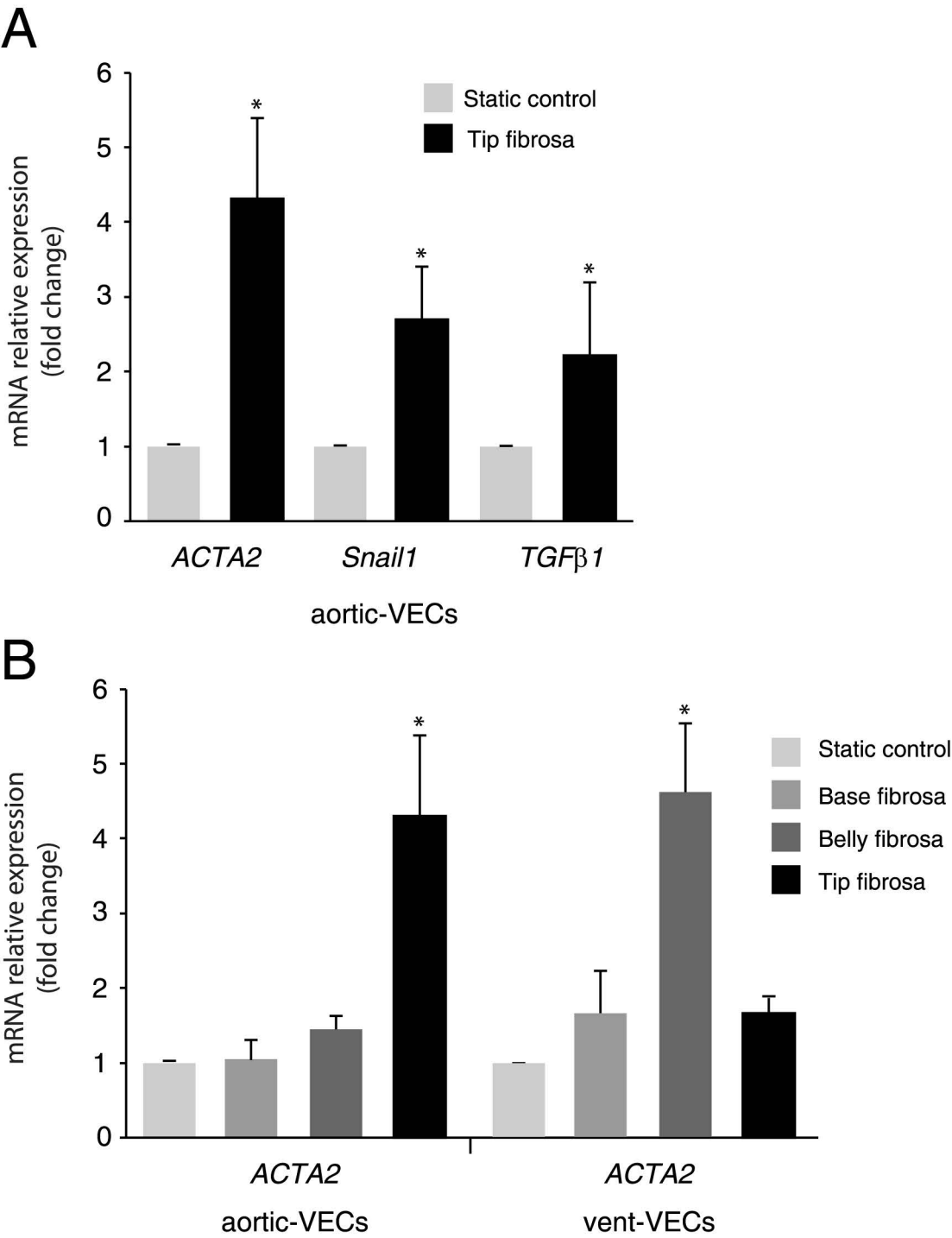
A
mRNA relative expression
(fold change)
0
1
2
3
4
5
6
Static control
Tip fibrosa
*
*
*
ACTA2
Snail1
TGFβ1
aortic-VECs
B
mRNA relative expression
(fold change)
0
1
2
3
4
5
6
Static control
Base fibrosa
Belly fibrosa
Tip fibrosa
*
*
ACTA2
ACTA2
aortic-VECs
vent-VECs

Figure 4

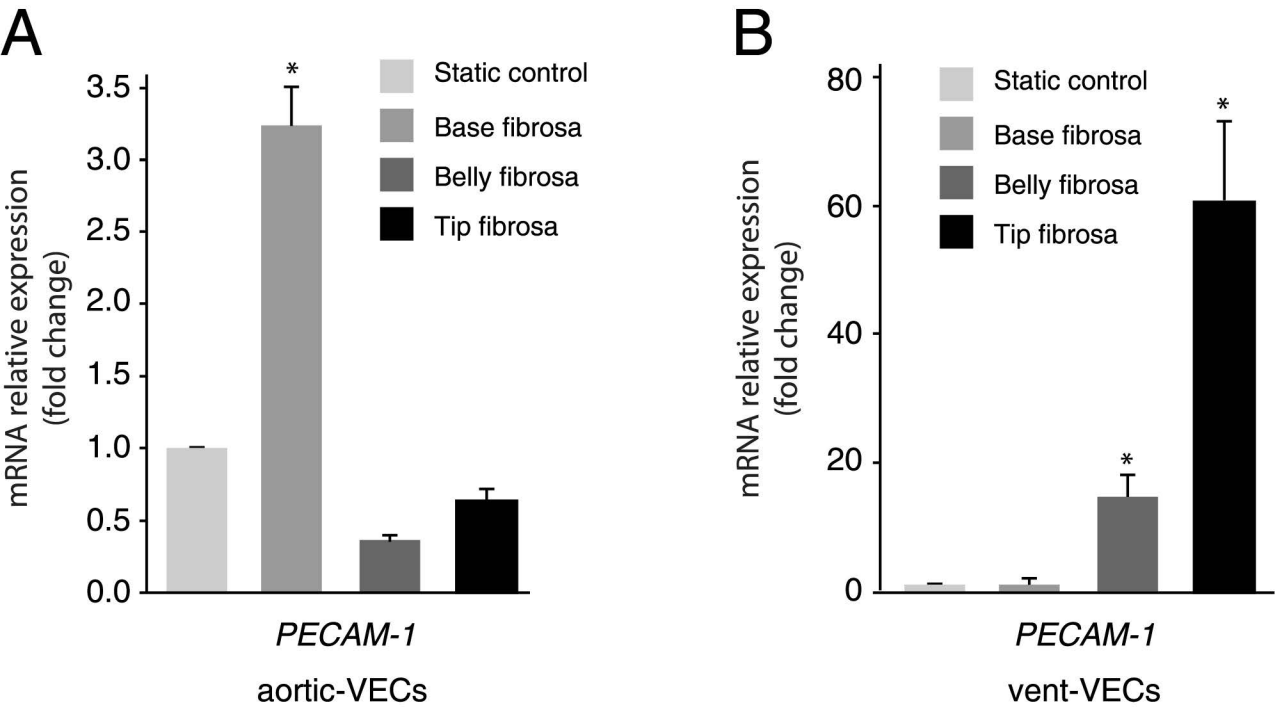
A
B
Static control
Base fibrosa
Belly fibrosa
Tip fibrosa
mRNA relative expression
(fold change)
3.5
3.0
2.5
2.0
1.5
1.0
0.5
0.0
80
60
40
20
0
*
PECAM-1
aortic-VECs
vent-VECs

Figure 5

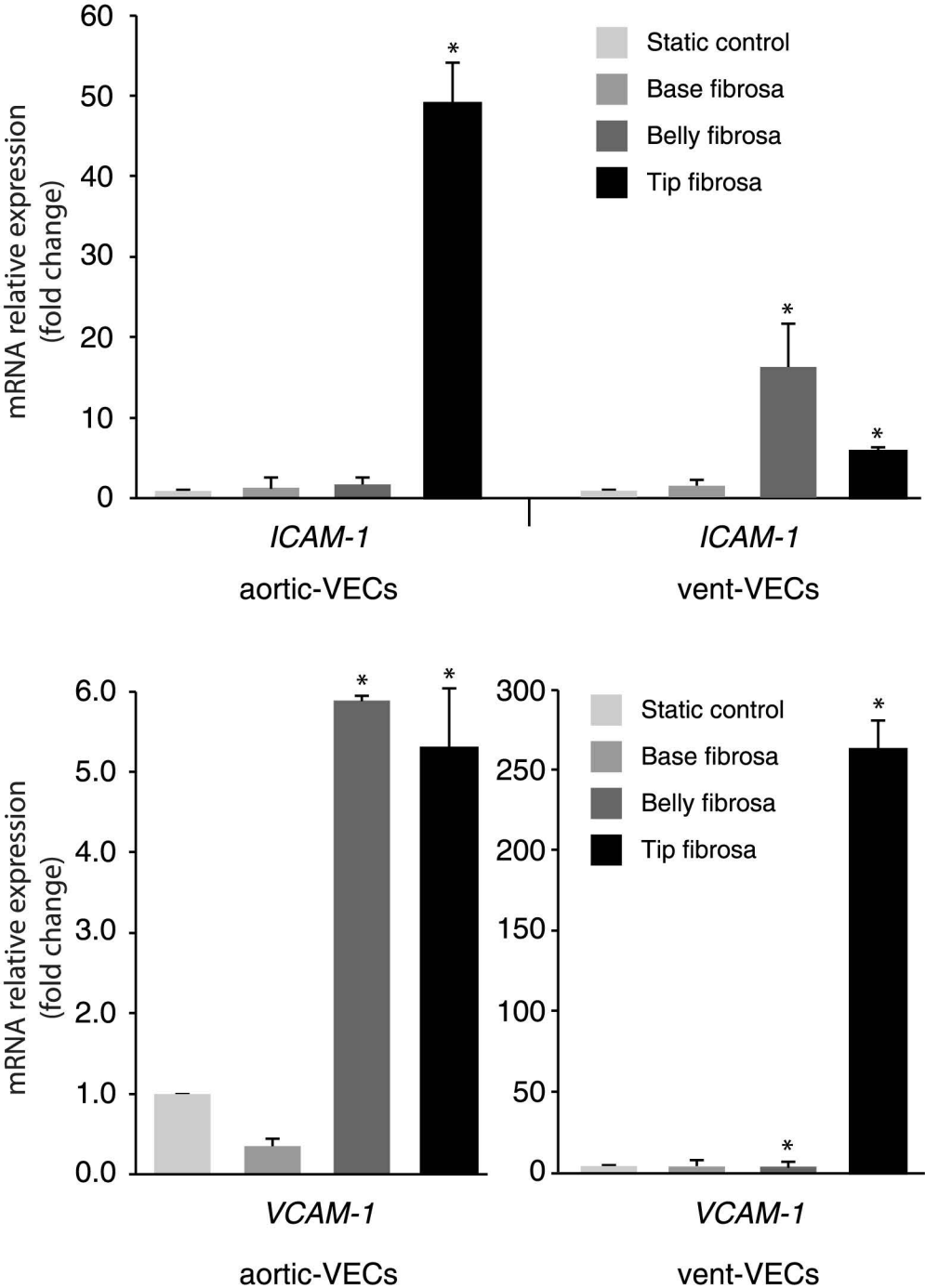
mRNA relative expression
(fold change)
60
50
40
30
20
10
0
Static control
Base fibrosa
Belly fibrosa
Tip fibrosa
*
*
*
ICAM-1
aortic-VECs
ICAM-1
vent-VECs
6.0
5.0
4.0
3.0
2.0
1.0
0.0
300
250
200
150
100
50
0
VCAM-1
aortic-VECs
VCAM-1
vent-VECs

Figure 6

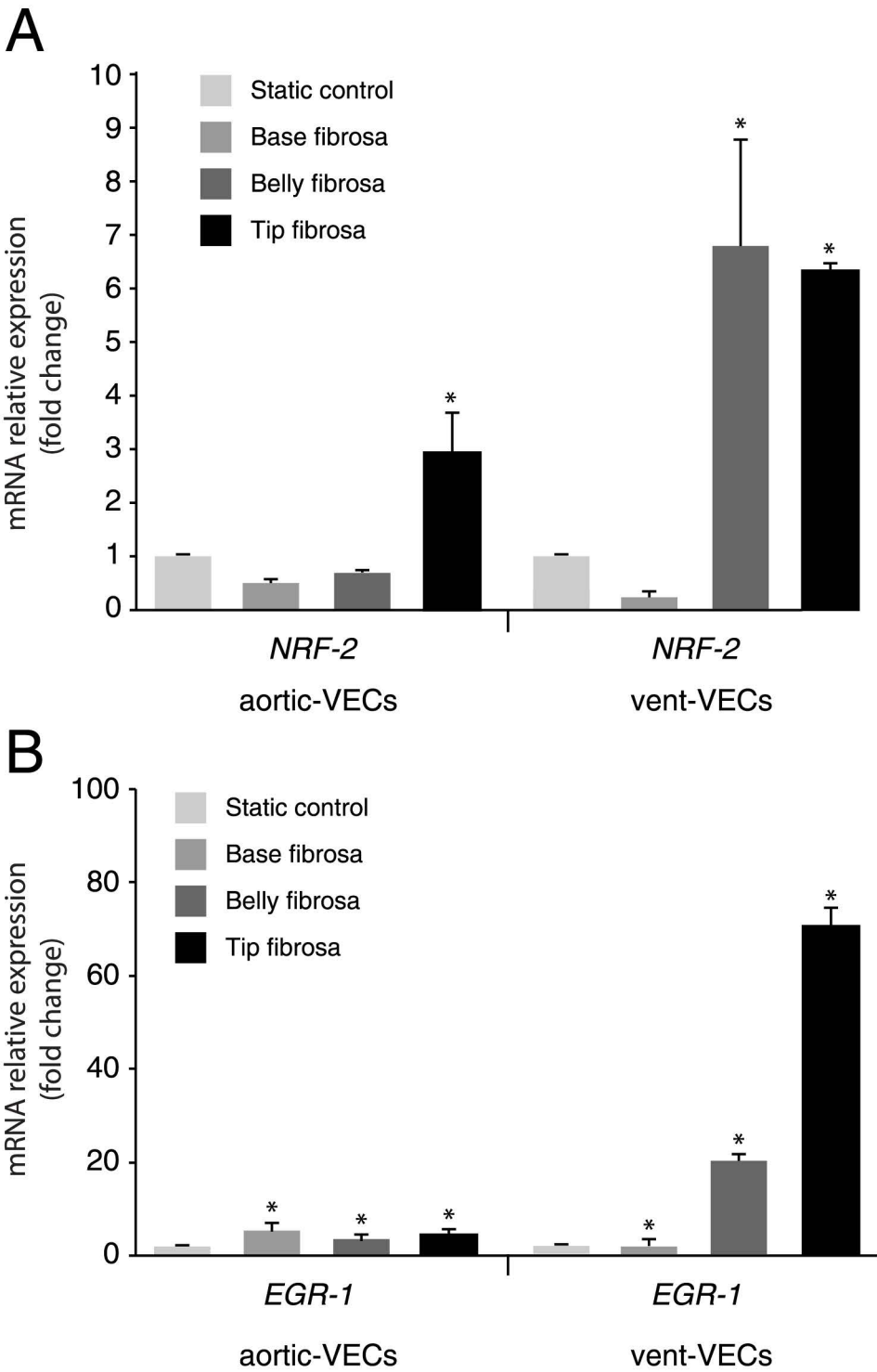
A
Static control
Base fibrosa
Belly fibrosa
Tip fibrosa
mRNA relative expression
(fold change)
10
9
8
7
6
5
4
3
2
1
0
*
*
*
NRF-2
aortic-VECs
NRF-2
vent-VECs
B
Static control
Base fibrosa
Belly fibrosa
Tip fibrosa
mRNA relative expression
(fold change)
100
80
60
40
20
0
*
*
*
*
*
*
EGR-1
aortic-VECs
EGR-1
vent-VECs

Figure 7